

## Temperature-Gradient-Driven Magnetic Skyrmion Motion

Eleonora Raimondo<sup>1</sup>, Elias Saugar,<sup>2</sup> Joseph Barker<sup>1</sup>, Davi Rodrigues<sup>1</sup>, Anna Giordano,<sup>5</sup> Mario Carpentieri,<sup>4</sup> Wanjun Jiang,<sup>6,7</sup> Oksana Chubykalo-Fesenko,<sup>2</sup> Riccardo Tomasello<sup>1,\*</sup>, and Giovanni Finocchio<sup>1,†</sup>

<sup>1</sup>*Department of Mathematical and Computer Sciences, Physical Sciences and Earth Sciences, University of Messina, I-98166 Messina, Italy*

<sup>2</sup>*Instituto de Ciencia de Materiales de Madrid, CSIC, Cantoblanco, 28049 Madrid, Spain*

<sup>3</sup>*School of Physics and Astronomy, University of Leeds, Leeds LS2 9JT, United Kingdom*

<sup>4</sup>*Department of Electrical and Information Engineering, Politecnico of Bari, 70125 Bari, Italy*

<sup>5</sup>*Department of Engineering, University of Messina, I-98166 Messina, Italy*

<sup>6</sup>*State Key Laboratory of Low-Dimensional Quantum Physics and Department of Physics, Tsinghua University, Beijing 100084, China*

<sup>7</sup>*Frontier Science Center for Quantum Information, Tsinghua University, Beijing 100084, China*



(Received 3 May 2022; revised 14 July 2022; accepted 14 July 2022; published 23 August 2022)

The static and dynamic properties of skyrmions have recently received increased attention due to the potential application of skyrmions as information carriers and for unconventional computing. While the current-driven dynamics has been explored deeply, both theoretically and experimentally, the theory of temperature gradient-induced dynamics—skyrmion caloritronics—is still at its early stages of development. Here, we move the topic forward by identifying the role of entropic torques due to the temperature dependence of magnetic parameters. Our results show that skyrmions move towards higher temperatures in single-layer ferromagnets with interfacial Dzyaloshinski-Moriya interactions, whereas, in multilayers, they move to lower temperatures. We analytically and numerically demonstrate that the opposite behaviors are due to different scaling relations of the material parameters as well as a non-negligible magnetostatic field gradient in multilayers. We also find a spatially dependent skyrmion Hall angle in multilayers hosting hybrid skyrmions due to variations of the thickness-dependent chirality as the skyrmion moves along the temperature gradient.

DOI: 10.1103/PhysRevApplied.18.024062

### I. INTRODUCTION

Magnetic skyrmions have been receiving increasing attention in the last decades. Since the initial theoretical studies and predictions on the fundamental and promising application properties of these “topologically protected” solitons [1–3], great efforts have been placed in material development for the experimental stabilization of skyrmions. The earliest experimental observations were in  $B_{20}$  compounds, where the bulk Dzyaloshinskii-Moriya interaction (DMI) promotes the formation of Bloch skyrmions [4–9]. Later, an increased effort has been devoted to thin films and heterostructures where ferromagnetic layers (FMs) are coupled with heavy metals (HMs), which are characterized by interfacial DMI (IDMI) [10]. These systems allow skyrmions to be stabilized at room temperature, which is a fundamental requirement

for practical applications. Lately, skyrmions have been reported in a variety of thin-film materials, including HM/single-layer FM/oxide [11–13], HM1/FM/HM2 multilayers [14–21], HM/ferrimagnet/oxide multilayers [22, 23], synthetic antiferromagnets (SAFs) [24–26], as well as bulk systems [27,28].

The standard approach to manipulate skyrmions is by electrical currents through the conventional spin-orbit torques (SOTs) [13,15,16,29–31]. However, alternative methods have been proposed, such as by external field [32,33] and perpendicular anisotropy [34] gradients as well as thermal gradients [35,36]. The manipulation by thermal gradients is particularly promising due to its low energy consumption, and is at the basis of a recent research direction named skyrmion caloritronics [35].

Thermal fluctuations have also been predicted to induce internal deformations, breathing excitations, and Brownian diffusion [37–41]. The latter has recently been experimentally observed and exploited in a low pinning material to design a reshuffle device for probabilistic computing

\*riccardo.tomasello@poliba.it

†gfinocchio@unime.it

[42]. Moreover, experiments have shown unidirectional diffusion of skyrmions in thermal gradients, where they moved from hot to cold regions [35]. This observation has been explained through the combination of repulsive forces between skyrmions, thermal SOTs [43], magnonic spin torques [44,45] as well as entropic forces. Recently, Gong *et al.* [46] proposed the existence of spin currents generated by thermal gradients to explain the observed skyrmion motion and concluded that skyrmions can move in either direction of the temperature gradient depending on the material parameters.

We have previously demonstrated the influence of thermal fluctuations on skyrmion stationary properties in single layers [40], through variations of the magnetic parameters (exchange, interfacial DMI, perpendicular anisotropy constants) whose scaling relations were obtained by atomistic calculations. However, that study did not consider the influence of thermal fluctuations on the skyrmion dynamical properties. Moreover, in a previous study [47] performed numerically and within Thiele's formalism [48], we have shown that a linear gradient of the perpendicular anisotropy generates skyrmion motion in a single-layer FM. We observed that the skyrmion exhibits a Hall effect with a major component of the velocity along the direction perpendicular to the anisotropy gradient, and a smaller velocity component (damping-dependent) in the same direction of the current. Furthermore, the adiabatic adjustment of the skyrmion size in the anisotropy gradient produces a uniform acceleration.

In this work, we study the effects of thermal gradients on skyrmion motion in different systems (single-layer FM with IDMI, multilayer, and SAF) inspired by the experimental results of Ref. [35] and from a fundamental point of view. We consider the previously obtained two-dimensional (2D) scaling relations to analyze the thermal gradient-driven skyrmion motion in a single layer with IDMI. Using atomistic simulations, we also compute the characteristic scaling relations for magnetic multilayers where several atomic layers are taken into account and the DMI is induced at both ferromagnet interfaces (for example Pt/FeCo/Ir [17,49] can be used as the active trilayer in  $N$  repetitions for a multilayer stack) and investigate the thermal gradient-driven motion of a skyrmion in these systems. In particular, we focus on two effects: the entropic torque and magnonic torque. The first one, already studied for domain walls [50], is analyzed in a deterministic scenario and is based on thermodynamic phenomena. It generates a skyrmion motion towards the region where its free energy is minimized. The second one occurs in a stochastic framework where thermal spin waves propagating from the hot to the cold region exert a torque on skyrmions by moving them in the opposite direction—from cold to hot [45]. We observe that, when driven by the entropic torque, skyrmions in single layers move from the cold to the hot region with a finite skyrmion

Hall angle, while in multilayers they move in the opposite direction (from hot to cold region). The numerical results are corroborated by a generalized Thiele's equation developed for this scenario, taking into account variations of the skyrmion size along its trajectory. Moreover, we show that the skyrmion Hall angle is completely suppressed in SAFs, similarly to the current-driven skyrmions [51–53]. The effect of the magnonic torque agrees with previous predictions [45] and induces the skyrmion motion towards the hotter region regardless of the system.

Our results have fundamental implications in the future development of skyrmionic devices combining thermal gradients and SOTs where the proper temperature dependence of the parameters should be taken into account. In addition, our work extends the application of controlled skyrmion motion to electric insulators and contributes to the design of waste-heat-recovery methods taking advantage of the thermal-driven skyrmion nucleation and shifting, promoting the field of skyrmion caloritronics.

## II. THEORETICAL MODELS

### A. Micromagnetic simulations

The micromagnetic computations are performed with a state-of-the-art micromagnetic solver, PETASPIN, which uses the Adams-Bashforth [54,55] method to numerically integrate the Landau-Lifshitz-Gilbert (LLG) equation:

$$\frac{d\mathbf{m}}{d\tau} = -(\mathbf{m} \times \mathbf{h}_{\text{eff}}) + \alpha_G \left( \mathbf{m} \times \frac{d\mathbf{m}}{d\tau} \right), \quad (1)$$

where  $\alpha_G$  is the Gilbert damping,  $\mathbf{m} = \mathbf{M}/M_S$  is the normalized magnetization vector, and  $\tau = \gamma_0 M_S t$  is the dimensionless time, with  $\gamma_0$  being the gyromagnetic ratio, and  $M_S$  the saturation magnetization.  $\mathbf{h}_{\text{eff}}$  is the effective magnetic field, which includes the exchange ( $A$ ), interfacial DMI (IDMI  $D$ ), uniaxial anisotropy ( $K_u$ ), magneto-static, and external fields ( $H_{\text{ext}}$ ) [21,56]. We simulate a squared  $1200 \times 1200 \text{ nm}^2$  sample for the single-layer FM, and a squared  $900 \times 900 \text{ nm}^2$  for the multilayer.

We include the change in saturation magnetization with temperature as  $M_S(T) = M_S(0)(1 - (T/T_{\text{lim}})^\delta)$  with  $M_S(0)$  being the saturation magnetization of the ferromagnet at zero temperature,  $\delta = 1.5$  and  $T_{\text{lim}} = 1120 \text{ K}$  is the Curie temperature [57–59].

We simulate three different systems: single-layer FM with IDMI, multilayer with five FM repetitions, and SAF. The parameters at zero temperature used for each of them are listed in Table I, while further details of the micromagnetic model can be found in Note S1 within the Supplemental Material [60].

For the macroscopic parameters, in a single-layer FM with IDMI, we use the 2D scaling relations from our

TABLE I. Summary of the micromagnetic parameters at zero temperature used in the simulations.

Parameter	Single-layer FM [61]	Multilayer	SAF
$M_S$ (kA/m)	1060	1300	770
$A$ (pJ/m)	20	15	20
$D$ (mJ/m <sup>2</sup> )	2.2	1.0	2.5
$K_u$ (MJ/m <sup>3</sup> )	0.90	1.20	0.60
Out-of-plane $H_{\text{ext}}$ (mT)	15	60	0

previous work [40], which are as follows:

$$\begin{aligned} A(T) &= A(0)m(T)^{\alpha}, \quad D(T) = D(0)m(T)^{\beta}, \\ K_u(T) &= K_u(0)m(T)^{\gamma}, \end{aligned} \quad (2)$$

where  $\alpha = \beta = 1.5$ ,  $\gamma = 3.0$ , and  $m(T) = M_S(T)/M_S(0)$ . For the Pt/FeCo/Ir trilayer, the scaling relations are evaluated by atomistic simulations, as shown below.

In the micromagnetic simulations, we use a linear thermal gradient from 100 to 300 K along the  $x$  direction. The minimum (maximum) value is considered on the left (right) side of the sample, where the corresponding maximum (minimum) value of the magnetic parameters are calculated from the scaling relations.

## B. Atomistic simulations

We use atomistic spin simulations to calculate the temperature dependence of magnetic parameters using the technique developed in Ref. [40]. We model the thin film as an fcc (111) lattice with two layers of Fe (adjacent to Ir), one layer of 50:50 mixed Fe and Co, and then two layers of Co (adjacent to Pt). The Hamiltonian is given by

$$H = \sum_{\langle ij \rangle} J_{ij} \mathbf{S}_i \cdot \mathbf{S}_j + \sum_{\langle ij \rangle} \mathbf{D}_{ij} \cdot (\mathbf{S}_i \times \mathbf{S}_j) - \sum_{\langle ij \rangle} K_{ij} S_{zi} S_{zj}, \quad (3)$$

where the first term is the isotropic exchange, the second is the DMI, which only occurs at the Ir-Fe and Co-Pt interfaces and the third is the two-ion anisotropy, which acts only at the Co-Pt interface. In this finite thickness film, the IDMI (and anisotropy) is only present at the Ir-Fe and Co-Pt interface layers whereas the exchange is present in and between all layers. The angle brackets,  $\langle ij \rangle$ , denote that we consider only nearest neighbors. We parametrize the exchange anisotropy and DMI constants using values from *ab initio* calculations in Ref. [17]  $J_{ij}$  (Fe - Fe) = 24.2 meV,  $J_{ij}$  (Co - Co) = 29.0 meV,  $J_{ij}$  (Fe - Co) = 26.6 meV,  $D_{ij}$  (Fe - Ir) = -0.854 meV,  $D_{ij}$  (Co - Pt) = 1.281 meV,  $K_{ij}$  (Co - Co) = 0.59 meV and use magnetic moments  $\mu(\text{Fe}) = 1.7\mu_B$  and  $\mu(\text{Co}) = 1.3\mu_B$  [62].

The temperature dependence of the anisotropy is calculated using the constrained Monte Carlo method [63]. The temperature dependence of exchange stiffness and IDMI is calculated from the softening [64] and shifting asymmetry of the spin-wave spectrum. The spectrum contains five bands and we fit the lowest band in the low  $k$  limit (see Supplemental Material of Ref. [40] for details of the technique).

We express the scaling relations in terms of the magnetization of the whole thin film, which corresponds to what is most accessible experimentally and is used in micromagnetic simulations for single layers. We find that the Ir/FeCo/Pt trilayer has the scaling parameters  $\alpha = 1.7$ ,  $\beta = 2.0$ , and  $\gamma = 2.5$ . This is different from in a 2D (atomic monolayer) system where the  $\alpha$  and  $\beta$  parameters are found to be identical [40,65]. Thus,  $\beta = 2.0$  and  $\gamma = 2.5$  are modified because their temperature dependence is dominated by spin fluctuations at interfaces that are different from the bulk where there is a different number of neighboring spins. This implies that, by changing the properties of the multilayer, including heavy metal materials and geometry, it is possible to tune the exponents  $\beta = 2.0$  and  $\gamma = 2.5$ . We note, however, that  $\alpha = 1.7$  is closer to the bulk value ( $\alpha = 1.8$ ) [66] than in the 2D case ( $\alpha = 1.5$ ) due to the finite thickness of the model considered. The exchange and DMI are also sensitive to different types of spin fluctuation, with  $A$  being mostly dependent on in-plane fluctuations whilst  $D$  is sensitive also to the out-of-plane fluctuations, which are different in the thicker and asymmetric system compared to the 2D case [65]. We emphasize, therefore, that the thickness of the film and the interface properties play a role overall on the temperature dependence of the material parameters.

## C. Generalized Thiele's equation

Despite the complex dynamics of the LLG Eq. (1), magnetic skyrmions are collective excitation states, which behave as particlelike objects with reduced degrees of freedom. This physical behavior is captured by Thiele's equation [48,67,68], which describes the motion of rigid magnetic textures. In order to include observed changes in the skyrmion size, we consider an adiabatic evolution of the skyrmion size such that at each instant the skyrmion motion is approximately described as a rigid object and the Thiele approach is still valid. It is worthwhile to notice, however, that within the range of material parameters and temperature gradient used in this paper, the skyrmion radius is approximately constant (see Note S2 within the Supplemental Material [60]). Within this approximation, the motion of the skyrmion at each instant is given by

$$\frac{d\mathbf{m}}{d\tau}(\mathbf{x}, \tau) = -\mathbf{v}(\mathbf{x}, \tau) \cdot \nabla \mathbf{m}(\mathbf{x}, \tau), \quad (4)$$

where  $\mathbf{v} = v_x \hat{\mathbf{x}} + v_y \hat{\mathbf{y}}$  is the velocity of the skyrmion center. By substituting Eq. (4) into Eq. (1) and projecting along  $\mathbf{m} \times \partial_i \mathbf{m}$ , with  $i = x, y$ , we obtain a generalized Thiele equation from which we derive the velocity of the skyrmion as

$$v_x = -\frac{4\pi\alpha_G D_{\text{ex}} F_x}{\alpha_G^2 D_{\text{ex}}^2 + (4\pi)^2} \text{ and } v_y = -\frac{4\pi F_x}{\alpha_G^2 D_{\text{ex}}^2 + (4\pi)^2}, \quad (5)$$

where  $D_{\text{ex}} = \int d^2x (\partial_x \mathbf{m} \cdot \partial_x \mathbf{m}) = \int d^2x (\partial_y \mathbf{m} \cdot \partial_y \mathbf{m})$  is the viscosity tensor components for a radially symmetric skyrmion, and  $F_x = -\partial_x V$ , with  $V(\mathbf{x}') = \int d^2x' (\mathbf{m}(\mathbf{x}', \tau) \cdot \mathbf{h}_{\text{eff}}(\mathbf{x}, \tau))$ , is the force due to a gradient in the effective field along the  $x$  axis. The size of the skyrmion, however, influences  $D_{\text{ex}}$  and  $F_x$ . The nonvanishing component  $v_y$  of the velocity perpendicular to the force  $F_x$  is due to the Magnus force experienced by the skyrmion and is associated with its topological charge [69]. Moreover, the velocity  $v_x$  along  $F_x$  is due to the influence of damping  $\alpha_G$ .

In the presence of a thermal gradient (expressed as the gradient of magnetic parameters) along the  $x$  direction, we obtain a dependence of the effective field  $\mathbf{h}_{\text{eff}}$  on the  $x$  coordinate, which in turn produces a motion of the skyrmion. For sufficiently large skyrmions (skyrmion radius  $R$  bigger than domain-wall width  $\Delta = \sqrt{A/K_{\text{eff}}}$ ), we can assume the following ansatz  $m_z = \arccos(2 \arctan((R/r)e^{\xi(R-r)}))$ , with  $\xi = (1/\Delta)\sqrt{2K_{\text{eff}}/\mu_0 M_S^2}$ , [40], and then we have that, in the limit of large skyrmions,

$$V = 2\pi\sigma_{\text{DW}}R + 2\pi M_S H_T R^2. \quad (6)$$

Here  $\sigma_{\text{DW}} \approx 4\sqrt{AK_{\text{eff}}} - \pi D$  is the domain-wall energy density [40, 67, 70, 71]. Notice that, for a magnetization saturation varying along the sample, the magnetostatic field cannot be fully incorporated into the renormalization via the effective anisotropy  $K_{\text{eff}}$ , and we include a contribution to the external field  $H_T = H_z - b\mu_0 M_S$ ,  $b$  depend on the properties of the film (for details see Note S2 within the Supplemental Material [60]). Thus, a gradient in temperature produces position-dependent material parameters  $A$ ,  $D$ ,  $K_u$ , and  $M_S$ , as well as, within an adiabatic approximation, a position-dependent size of the skyrmion and

generates the motion of the skyrmion with a nonconstant velocity. Furthermore, we emphasize that the change in the saturation magnetization  $M_S$  along the film due to the temperature gradient also produces a stray field gradient. This effect can be incorporated into the effective anisotropy (thin-film approximation) for the case of the single layer, however the thin-film approximation does not hold for the multilayer. Therefore, in Thiele's equation for the multilayer, the non-negligible stray field gradient is considered through a perpendicular external field gradient.

### III. RESULTS

#### A. Single-layer FM and multilayer

Figure 1 shows the main result of this work, which is obtained from deterministic micromagnetic simulations when a linear gradient of temperature is considered for the single-layer FM and the multilayer. Surprisingly, the trajectory of the skyrmion (here we consider the position of the skyrmion given by the  $x$ - $y$  position of the skyrmion core, calculated as the geometrical center of the circular region enclosed within  $m_z \leq 0$ ), is qualitatively opposite for the two cases. In the single-layer FM [Fig. 1(a)], the skyrmion moves with positive velocities in the  $x$  and  $y$  directions, i.e., towards the region with higher temperature. Whereas, in the multilayer case [Fig. 1(b)], it has negative velocities, with respect to the  $x$  and  $y$  directions, i.e., it moves towards the colder region. The latter is a particularly interesting outcome due to the qualitative agreement with the experimental observations of skyrmion motion driven by linear thermal gradients in magnetic multilayers [see Fig. 3(a) in Ref. [35]].

To understand the origin of such a different behavior, we perform a detailed analysis combining full numerical simulations and Thiele's equation.

When considering a deterministic approach with linear gradient of the micromagnetic parameters, the skyrmion moves towards the parameters region where its energy is minimized. In particular, in this work, the energy minimization as a function of temperature leads the skyrmion radius to expand. Therefore, the effect that each micromagnetic parameter gradient has on the skyrmion motion can

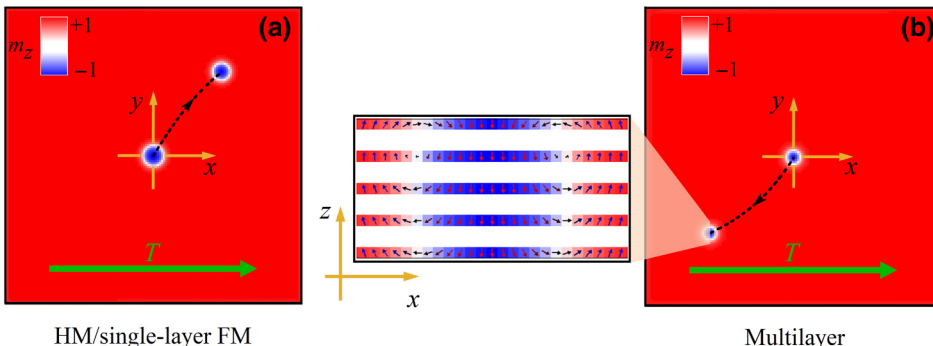


FIG. 1. Trajectory of the skyrmion induced by a linear gradient of temperature in a (a) single FM with IDMI, and (b) multilayer with five FM repetitions. The magnification of the skyrmion in (b) shows the cross section along the multilayer thickness that highlights the existence of a hybrid skyrmion [21].

TABLE II. Summary of the trajectories of the skyrmion motion under a linear gradient of the parameters.

Parameter gradient	Single-layer FM	Multilayer
$M_S$	$v_x < 0, v_y < 0$ (motion to the cold region)	$v_x < 0, v_y < 0$ (motion to the cold region)
$A$	$v_x > 0, v_y > 0$ (motion to the hot region)	$v_x > 0, v_y > 0$ (motion to the hot region)
$D$	$v_x < 0, v_y < 0$ (motion to the cold region)	See discussion of Fig. 3 below
$K_u$	$v_x > 0, v_y > 0$ (motion to the hot region)	$v_x > 0, v_y > 0$ (motion to the hot region)

be straightforwardly deduced since in this case it will move towards the region where the local value of the parameter favors the existence of a larger skyrmion. To confirm the previous qualitative argument, we perform systematic simulations in which the gradients of the parameters are considered independently both in the single-layer FM and multilayer. The results are summarized in Table II, while the different trajectories are shown in Note S3 within the Supplemental Material [60]. The perpendicular anisotropy and exchange parameters' gradients promote the skyrmion motion to the region where those parameters are smaller, therefore from the cold to the hot region. In contrast, the  $M_S$  (magnetostatic field),  $D$  and the combination of  $M_S$  and  $A$  gradients, move the skyrmion to the region where those parameters are larger, thus from the hot to the cold region. This can be understood from Eq. (6) and directly from the domain-wall energy density  $\sigma_{DW}$  [70,72]. It is clear that the skyrmion energy increases as  $A$  and  $K$  increase, while it decreases for higher  $M_S$  and  $D$  (the scenario is more complicated for the multilayer, as discussed below).

When considering the combinations of all parameters' gradient due to a thermal gradient, the scenario becomes complex and the final effect on skyrmion motion depends on their values. Figure 1 suggests that the direction of skyrmion motion results from which of the antagonistic effects ( $A$  and  $K_u$ , or IDMI and  $M_S$ ) is dominant.

First, we focus on the single-layer FM. Figure 1(a) entails that the 2D scaling relations lead to the dominance of  $A$  and  $K_u$  parameters over IDMI and  $M_S$ . To better understand and control this behavior, we must consider 2 degrees of freedom: (i) the change of the scaling exponents, and (ii) different zero temperature values of the magnetic parameters. We focus on the IDMI scaling relation since the value of the IDMI can be easily tuned by modifying the materials, i.e., using different heavy metals and modifying their thickness [73], at the ferromagnetic

interfaces (see Sec. II B) without a significant change of other material parameters. By fixing the scaled values of the other parameters as well as the zero temperature value of the IDMI, we carry out a systematic study of the skyrmion trajectory as a function of the scaling exponent  $\beta$  (the range of values for  $\beta$  are chosen such that the radially symmetric skyrmions are still stable). Figure 2(a) shows the results where, for  $1.5 \leq \beta \leq 2.7$ , the skyrmions preserves its motion towards the hot region, similarly to Fig. 1(a), whereas, in the range  $2.8 \leq \beta \leq 4.0$ , the motion is reversed and the skyrmion moves towards the cold region. In other words, there exists a threshold value of the exponent  $\beta$ , which determines the motion of the skyrmion to the cold region, albeit the DMI should decay with magnetization quite fast.

Figure 2(b) illustrates the skyrmion motion when we fix two values of  $\beta = 4.0$  and  $1.5$ , respectively, for the left and right side of the figure, together with the scaled values of the other parameters and changed the zero-temperature value of the IDMI,  $D(0)$ . In both cases, the skyrmion trajectory is barely affected by  $D(0)$ . Therefore, we conclude that a strategy to control the direction of the skyrmion

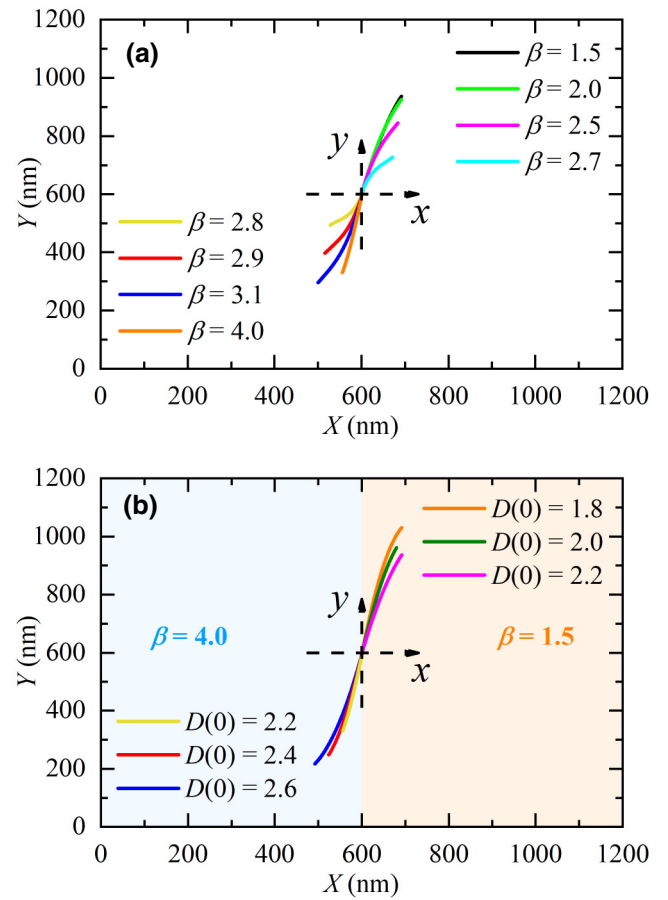


FIG. 2. (a) Trajectories of the skyrmion as a function of different  $\beta$ . (b) Trajectories of the skyrmion as a function of different  $D(0)$  for  $\beta = 1.5$  and  $\beta = 4.0$ , respectively.

motion is to properly tune the scaling exponent of the IDMI parameter (see Sec. II B).

We also perform a systematic study on the effect of the magnitude of the thermal gradient on the skyrmion velocity, which increases with the gradient as expected (see Note S4 within the Supplemental Material [60]).

Once the behavior in the single layer is fully understood, we proceed with the magnetic multilayer to understand the source of the skyrmion motion towards the colder region. In magnetic multilayers, skyrmions are characterized by an additional degree of freedom linked to the thickness-dependent chirality [21,49,74], which can be modified by tuning the IDMI parameter. It is well documented that an increase of the IDMI parameter on the hybrid skyrmion profile shifts the central Bloch skyrmion towards one of the most external layers, according to the IDMI sign [21,74]. Hence, we expect that, when considering a linear variation of  $D$ , the hybrid skyrmion profile changes along the gradient. It is useful to investigate whether this effect influences the skyrmion trajectory. Thus, we fix the IDMI gradient from 0 to  $-2 \text{ mJ/m}^2$ , such that in the center of the sample—corresponding to the  $x-y$  plane—the IDMI is given by  $D = -1.0 \text{ mJ/m}^2$ . In this case, we consider an IDMI gradient. At zero IDMI, static simulations show a symmetric hybrid skyrmion (see Note S1 within the Supplemental Material [60]), where the Bloch skyrmion is exactly in the middle layer.

Figure 3(a) depicts the hybrid skyrmion trajectory due to the IDMI gradient. We notice a change of slope when

the  $x$  position is around 540 nm. To understand the origin of such a change, we compute the helicity of the skyrmion, i.e., the in-plane angle of the magnetization vector at the boundary of the skyrmion (region where  $m_z = 0$ ) as illustrated in the inset of Fig. 3(b). An angle of  $90^\circ$  corresponds to a Bloch skyrmion, while an angle of  $0^\circ$  ( $180^\circ$ ) corresponds to a Néel skyrmion. The initial hybrid skyrmion is placed at the center of the sample in the  $x-y$  plane, where we expect the finite value of  $D$  to promote the shift of the Bloch skyrmion downward. This is evident from the cross-section S1. Therefore, we calculate the angle for the skyrmion placed in the second layer of the five-repeats multilayer. The initial angle is about  $107^\circ$  in Fig. 3(b), larger than  $90^\circ$  still due to the finite value of  $D$ , which tilts the Bloch chirality towards a Néel inward chirality. As the skyrmion moves towards larger values of  $|D|$ , the angle tends to approach  $180^\circ$ , which implies that the Bloch skyrmion has been shifted more downward being replaced by a Néel skyrmion with inward chirality. Our outcomes are also confirmed by the cross-section views S2–S5 in Fig. 3. By comparing the change of the slope in Fig. 3(a) with the corresponding angle in Fig. 3(b), we can conclude that the variation of the trajectory originates from the change of the thickness-dependent chirality of the hybrid skyrmion. This finding represents the second main result of this work.

However, the change of the skyrmion profile and helicity is not enough to justify the different behaviors observed between the single-layer FM and the multilayer. Indeed,

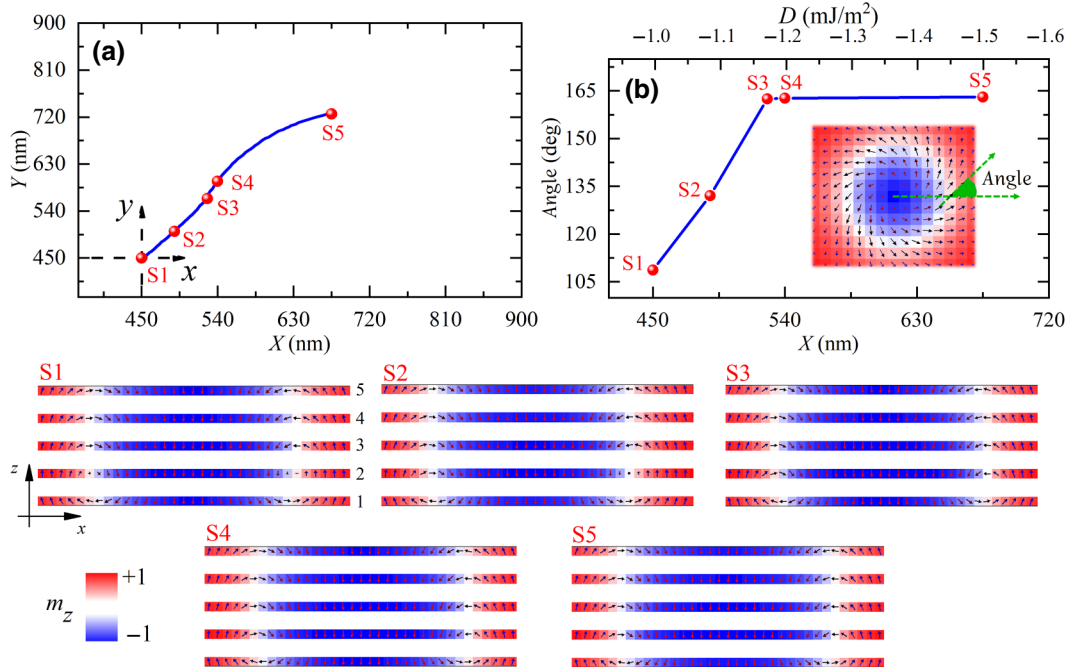
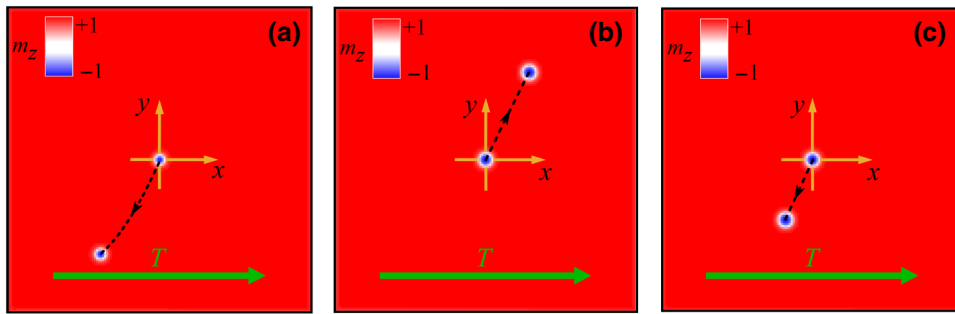


FIG. 3. (a) Skyrmion trajectory under a linear gradient of IDMI. (b) Angle of the magnetization vector of the skyrmion placed in the second layer of the five-repeats multilayer as a function of the  $x$  position of the skyrmion core. Inset: example of skyrmions where the angle of the magnetization vector is indicated. The S1–S5 points in (a),(b) are linked to the cross-section views below.



to exclude these effects, we perform a simulation fixing the thickness-dependent chirality during the motion, and still observe the skyrmion motion in the multilayer system towards the colder region.

Beyond the DMI contribution, another factor, which influences the dynamics in the two systems are the different scaling exponents. As a “numerical experiment,” we perform a micromagnetic simulation with a single layer, similar to the one in Fig. 1(a), and used the scaling relations obtained for the multilayer system (see Sec. II B). In this simulation, we observe that the Néel skyrmion moves towards the colder region [Fig. 4(a)], similarly to the hybrid skyrmion in multilayers. This unequivocally confirms the crucial role of the scaling relations that, for multilayers, leads to the dominance of the effect of the IDMI over the other parameters.

To corroborate our analysis in the single-layer FM simulations, we verify the behavior by using Thiele’s equation (see Sec. II C). Figures 4(b) and 4(c) show the skyrmion trajectory within the Thiele formalism for the single-layer FM and multilayer systems, respectively, where the skyrmion behavior is in excellent agreement with the full micromagnetic simulations. Notice that, the enhancement of the external field term proportional to  $\mu_0 M_s$  [see Eq. (6)] is not relevant for the skyrmion trajectory for the single-layer scaling relations while it is essential for multilayer case. In fact, as a further “numerical experiment” we perform a micromagnetic simulation with a single layer and scaling relations of the multilayer but without considering the extra contribution to the external field (i.e.,  $b = 0$ ). The skyrmion now changes direction and moves to the hotter region, likewise the case of the single-layer FM. This outcome points out that the gradient of the magnetostatic field in multilayers has a crucial effect in determining the skyrmion motion towards the colder region. For a detailed discussion on the forces for each case according to the Thiele formalism see Note S2 within the Supplemental Material [60].

Once the influence of the entropic torques are well understood, we analyze the effect of the magnonic torque. We perform stochastic micromagnetic simulations (see Note S5 within the Supplemental Material [60]) with a linear thermal field [75,76] gradient from 0 to 100 K. The skyrmion moves towards the hot region, similarly to

FIG. 4. Skyrmion trajectory under thermal gradient calculated for (a) a single FM layer with the scaling relations of the multilayer via micromagnetic simulations, and via Thiele’s equation with the scaling relations of the (b) single-layer FM, and (c) multilayer.

Fig. 1(a) and to previous reports [45], but with a stochastic dispersion of the Hall angle around its average value due to thermal fluctuations. These results are similar even for the case when magnonic torque and entropic torque (scaling relations of the parameters) are considered simultaneously.

## B. SAF

In a SAF, two skyrmions of opposite topological charges are antiferromagnetically coupled via the interlayer exchange coupling [52,77–79], and a vanishing skyrmion Hall effect is achieved [51,52,80]. Therefore, we expect the linear gradient-driven skyrmion motion to occur only in the direction of the gradients ( $x$  axis). This can be explained by the fact that in this case, the two coupled skyrmions experience Magnus forces of the same magnitude in opposite directions, such that the total

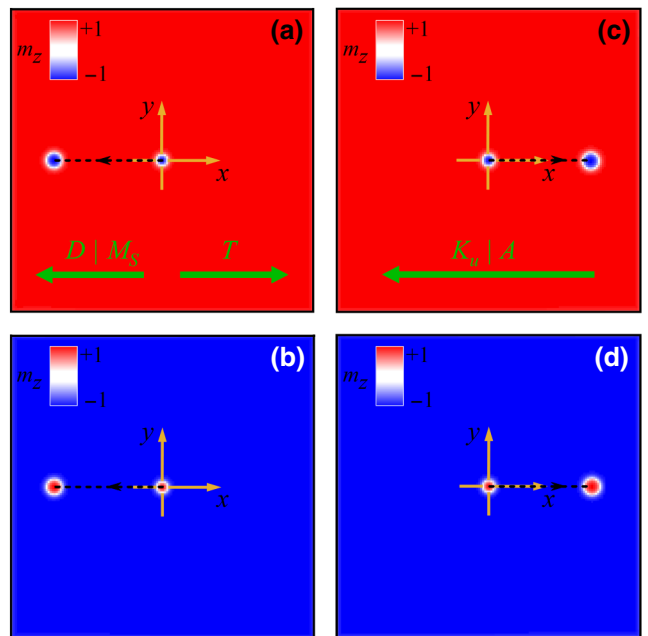


FIG. 5. (a),(b) Skyrmion trajectory under a linear gradient of IDMI (or  $M_s$ ) or thermal gradient, in the top layer and in the bottom layer of the SAF, respectively. (c),(d) Skyrmion trajectory under a linear gradient of  $K_u$  (or  $A$ ), in the top layer and in the bottom layer of the SAF, respectively.

net force perpendicular to perturbation vanishes, as in the case of spin-current-driven antiferromagnetic Néel skyrmions [51].

Our calculations show that the results obtained above on ferromagnetic systems are still valid for SAFs, where, according to the material choice, either single layer or multilayer scaling relations can be used. In the following, we show only the results with scaling relation of the multilayer.

Figures 5(a) and 5(b) show the motion direction due to the gradients IDMI,  $M_s$ , or thermal gradients, while Figs. 5(c) and 5(d) show the opposite direction of motion due to  $K_u$  or  $A$  gradients. In all the cases, the skyrmion is characterized by a zero Hall angle, but the entropic torque due to the thermal gradients [Figs. 5(a) and 5(b)] promotes the motion towards the cold region. Here, notice that the magnetostatic field gradient does not play any role because the SAF system has no stray field.

#### IV. SUMMARY AND CONCLUSIONS

In summary, we analyze the effect of linear thermal gradients on the skyrmion motion in single and multilayered thin films with interfacial DMI parameter in different systems through micromagnetic simulations and the Thiele formalism. We focus on the role of the entropic and magnonic torques. The former originates from the temperature dependence of the magnetic parameters, which scale with temperature. We observe opposite skyrmion motion directions in a single-layer FM and a multilayer. In the single-layer case, the skyrmion moves to the hotter region, whereas, in the multilayer case, the skyrmion moves towards the colder region, in qualitative agreement with experimental results [35]. We attribute this difference to the distinct scaling relations characterizing the two systems, and to the existence of a magnetostatic field gradient linked to the variation of  $M_s$ , which cannot be neglected in magnetic multilayers. We also show that the magnonic torque promotes the skyrmion motion towards the hotter region with stochastic dispersion of the trajectories around averaged Hall angle. In a SAF, the skyrmion motion due to the entropic torque occurs with a zero Hall angle towards either the colder or the hotter region according to the scaling relations considered.

Our results show the importance of the design of proper temperature dependence of the magnetic parameters and can have a fundamental impact in the future development and design of skyrmion devices in the field of skyrmion caloritronics.

#### ACKNOWLEDGMENTS

This work is supported by Project No. PRIN 2020LWPKH7 funded by the Italian Ministry of University and Research, and by the PETASPIN association ([www.petaspin.com](http://www.petaspin.com)). J.B. acknowledges support from

the Royal Society through a University Research Fellowship. Work carried out at Tsinghua is supported by the Basic Science Center Project of NSFC (Grant No. 51788104), Beijing Natural Science Foundation (Grant No. Z190009), the National Natural Science Foundation of China (Grants No. 11774194 and No. 51831005), the Beijing Advanced Innovation Center for Future Chip (ICFC). The work of E.S. and O.C.-F. was supported by the grants PID2019-108075RB-C31 funded by Ministry of Science and Innovation MCIN/AEI/10.13039/501100011033 and S2018/NMT-4321 NANOMAGCOST-CM funded by the Government of Madrid Region, Spain. We would like to acknowledge networking support from the COST Action No. CA17123 (MAGNETOFON) “Ultrafast opto magneto electronics for nondissipative information technology. In particular, E.R. acknowledges the economical support of MAGNETOFON within the STSM program.

- [1] N. Nagaosa and Y. Tokura, Topological properties and dynamics of magnetic skyrmions, *Nat. Nanotechnol.* **8**, 899 (2013).
- [2] A. Fert, V. Cros, and J. Sampaio, Skyrmions on the track, *Nat. Nanotechnol.* **8**, 152 (2013).
- [3] G. Finocchio, F. Büttner, R. Tomasello, M. Carpentieri, and M. Kläui, Magnetic skyrmions: From fundamental to applications, *J. Phys. D: Appl. Phys.* **49**, 423001 (2016).
- [4] S. Mühlbauer, B. Binz, F. Jonietz, C. Pfleiderer, A. Rosch, A. Neubauer, R. Georgii, and P. Boni, Skyrmion lattice in a chiral magnet, *Science* **323**, 915 (2009).
- [5] A. Neubauer, C. Pfleiderer, B. Binz, A. Rosch, R. Ritz, P. G. Niklowitz, and P. Böni, Topological Hall Effect in the  $A$  Phase of MnSi, *Phys. Rev. Lett.* **102**, 186602 (2009).
- [6] X. Z. Yu, Y. Onose, N. Kanazawa, J. H. Park, J. H. Han, Y. Matsui, N. Nagaosa, and Y. Tokura, Real-space observation of a two-dimensional skyrmion crystal, *Nature* **465**, 901 (2010).
- [7] S. X. Huang and C. L. Chien, Extended Skyrmion Phase in Epitaxial FeGe(111) Thin Films, *Phys. Rev. Lett.* **108**, 267201 (2012).
- [8] F. Zheng, F. N. Rybakov, A. B. Borisov, D. Song, S. Wang, Z.-A. Li, H. Du, N. S. Kiselev, J. Caron, A. Kovács, M. Tian, Y. Zhang, S. Blügel, and R. E. Dunin-Borkowski, Experimental observation of chiral magnetic bobbers in B20-type FeGe, *Nat. Nanotechnol.* **13**, 451 (2018).
- [9] A. S. Ahmed, J. Rowland, B. D. Esser, S. R. Dunsiger, D. W. McComb, M. Randeria, and R. K. Kawakami, Chiral bobbers and skyrmions in epitaxial FeGe/Si(111) films, *Phys. Rev. Mater.* **2**, 041401 (2018).
- [10] A. Soumyanarayanan, N. Reyren, A. Fert, and C. Panagopoulos, Emergent phenomena induced by spin-orbit coupling at surfaces and interfaces, *Nature* **539**, 509 (2016).
- [11] W. Jiang, P. Upadhyaya, W. Zhang, G. Yu, M. B. Jungfleisch, F. Y. Fradin, J. E. Pearson, Y. Tserkovnyak, K. L. Wang, O. Heinonen, S. G. E. te Velthuis, and A. Hoffmann, Blowing magnetic skyrmion bubbles, *Science* **349**, 283 (2015).

- [12] O. Boulle, J. Vogel, H. Yang, S. Pizzini, D. de S. Chaves, A. Locatelli, T. O. M. A. Sala, L. D. Buda-Prejbeanu, O. Klein, M. Belmeguenai, Y. Roussigné, A. Stashkevich, S. M. Chérif, L. Aballe, M. Foerster, M. Chshiev, S. Auffret, I. M. Miron, and G. Gaudin, Room temperature chiral magnetic skyrmion in ultrathin magnetic nanostructures, *Nat. Nanotechnol.* **11**, 449 (2016).
- [13] W. Jiang, X. Zhang, G. Yu, W. Zhang, X. Wang, M. Benjamin Jungfleisch, J. E. Pearson, X. Cheng, O. Heinonen, K. L. Wang, Y. Zhou, A. Hoffmann, and S. G. E. te Velthuis, Direct observation of the skyrmion Hall effect, *Nat. Phys.* **13**, 162 (2016).
- [14] C. Moreau-Luchaire, C. Moutafis, N. Reyren, J. Sampaio, C. A. F. Vaz, N. Van Horne, K. Bouzehouane, K. Garcia, C. Deranlot, P. Warnicke, P. Wohlhüter, J.-M. George, M. Weigand, J. Raabe, V. Cros, and A. Fert, Additive interfacial chiral interaction in multilayers for stabilization of small individual skyrmions at room temperature, *Nat. Nanotechnol.* **11**, 444 (2016).
- [15] S. Woo, K. Litzius, B. Krüger, M.-Y. Im, L. Caretta, K. Richter, M. Mann, A. Krone, R. M. Reeve, M. Weigand, P. Agrawal, I. Lemesh, M.-A. Mawass, P. Fischer, M. Kläui, and G. S. D. Beach, Observation of room-temperature magnetic skyrmions and their current-driven dynamics in ultrathin metallic ferromagnets, *Nat. Mater.* **15**, 501 (2016).
- [16] K. Litzius, I. Lemesh, B. Krüger, P. Bassirian, L. Caretta, K. Richter, F. Büttner, K. Sato, O. A. Tretiakov, J. Förster, R. M. Reeve, M. Weigand, I. Bykova, H. Stoll, G. Schütz, G. S. D. Beach, and M. Kläui, Skyrmion Hall effect revealed by direct time-resolved x-ray microscopy, *Nat. Phys.* **13**, 170 (2016).
- [17] A. Soumyanarayanan, M. Raju, A. L. Gonzalez Oyarce, A. K. C. Tan, M.-Y. Im, A. P. Petrović, P. Ho, K. H. Khoo, M. Tran, C. K. Gan, F. Ernult, and C. Panagopoulos, Tunable room-temperature magnetic skyrmions in Ir/Fe/Co/Pt multilayers, *Nat. Mater.* **16**, 898 (2017).
- [18] F. Büttner, I. Lemesh, M. Schneider, B. Pfau, C. M. Günther, P. Hessing, J. Geilhufe, L. Caretta, D. Engel, B. Krüger, J. Viehhaus, S. Eisebitt, and G. S. D. Beach, Field-free deterministic ultrafast creation of magnetic skyrmions by spin-orbit torques, *Nat. Nanotechnol.* **12**, 1040 (2017).
- [19] K. Zeissler, S. Finizio, K. Shahbazi, J. Massey, F. Al Ma'Mari, D. M. Bracher, A. Kleibert, M. C. Rosamond, E. H. Linfield, T. A. Moore, J. Raabe, G. Burnell, and C. H. Marrows, Discrete Hall resistivity contribution from Néel skyrmions in multilayer nanodisks, *Nat. Nanotechnol.* **13**, 1161 (2018).
- [20] D. Maccariello, W. Legrand, N. Reyren, K. Garcia, K. Bouzehouane, S. Collin, V. Cros, and A. Fert, Electrical detection of single magnetic skyrmions in metallic multilayers at room temperature, *Nat. Nanotechnol.* **13**, 233 (2018).
- [21] W. Li, *et al.*, Anatomy of skyrmionic textures in magnetic multilayers, *Adv. Mater.* **31**, 1807683 (2019).
- [22] S. Woo, K. M. Song, X. Zhang, Y. Zhou, M. Ezawa, X. Liu, S. Finizio, J. Raabe, N. J. Lee, S.-I. Kim, S.-Y. Park, Y. Kim, J.-Y. Kim, D. Lee, O. Lee, J. W. Choi, B.-C. Min, H. C. Koo, and J. Chang, Current-driven dynamics and inhibition of the skyrmion Hall effect of ferrimagnetic skyrmions in GdFeCo films, *Nat. Commun.* **9**, 959 (2018).
- [23] L. Caretta, M. Mann, F. Büttner, K. Ueda, B. Pfau, C. M. Günther, P. Hessing, A. Churikova, C. Klose, M. Schneider, D. Engel, C. Marcus, D. Bono, K. Bagschik, S. Eisebitt, and G. S. D. Beach, Fast current-driven domain walls and small skyrmions in a compensated ferrimagnet, *Nat. Nanotechnol.* **13**, 1154 (2018).
- [24] T. Dohi, S. DuttaGupta, S. Fukami, and H. Ohno, Formation and current-induced motion of synthetic antiferromagnetic skyrmion bubbles, *Nat. Commun.* **10**, 5153 (2019).
- [25] W. Legrand, D. Maccariello, F. Ajejas, S. Collin, A. Vecchiola, K. Bouzehouane, N. Reyren, V. Cros, and A. Fert, Room-temperature stabilization of antiferromagnetic skyrmions in synthetic antiferromagnets, *Nat. Mater.* **19**, 34 (2020).
- [26] R. Juge, *et al.*, Skyrmions in synthetic antiferromagnets and their nucleation via electrical current and ultrafast laser illumination, arxiv:2111, 1 (2021).
- [27] X. Yu, D. Morikawa, Y. Tokunaga, M. Kubota, T. Kurumaji, H. Oike, M. Nakamura, F. Kagawa, Y. Taguchi, T. Arima, M. Kawasaki, and Y. Tokura, Current-induced nucleation and annihilation of magnetic skyrmions at room temperature in a chiral magnet, *Adv. Mater.* **29**, 1606178 (2017).
- [28] W. Wang, D. Song, W. Wei, P. Nan, S. Zhang, B. Ge, M. Tian, J. Zang, and H. Du, Electrical manipulation of skyrmions in a chiral magnet, *Nat. Commun.* **13**, 1593 (2022).
- [29] W. Legrand, D. Maccariello, N. Reyren, K. Garcia, C. Moutafis, C. Moreau-Luchaire, S. Collin, K. Bouzehouane, V. Cros, and A. Fert, Room-temperature current-induced generation and motion of sub-100 nm skyrmions, *Nano Lett.* **17**, 2703 (2017).
- [30] G. Yu, P. Upadhyaya, Q. Shao, H. Wu, G. Yin, X. Li, C. He, W. Jiang, X. Han, P. K. Amiri, and K. L. Wang, Room-temperature skyrmion shift device for memory application, *Nano Lett.* **17**, 261 (2017).
- [31] K. Zeissler, S. Finizio, C. Barton, A. J. Huxtable, J. Massey, J. Raabe, A. V. Sadovnikov, S. A. Nikitov, R. Brearton, T. Hesjedal, G. van der Laan, M. C. Rosamond, E. H. Linfield, G. Burnell, and C. H. Marrows, Diameter-independent skyrmion Hall angle observed in chiral magnetic multilayers, *Nat. Commun.* **11**, 428 (2020).
- [32] S. L. Zhang, W. W. Wang, D. M. Burn, H. Peng, H. Berger, A. Bauer, C. Pfleiderer, G. van der Laan, and T. Hesjedal, Manipulation of skyrmion motion by magnetic field gradients, *Nat. Commun.* **9**, 2115 (2018).
- [33] A. Casiraghi, H. Corte-León, M. Vafaei, F. García-Sánchez, G. Durin, M. Pasquale, G. Jakob, M. Kläui, and O. Kazakova, Individual skyrmion manipulation by local magnetic field gradients, *Commun. Phys.* **2**, 145 (2019).
- [34] G. Yu, P. Upadhyaya, X. Li, W. Li, S. K. Kim, Y. Fan, K. L. Wong, Y. Tserkovnyak, P. K. Amiri, and K. L. Wang, Room-temperature creation and spin-orbit torque manipulation of skyrmions in thin films with engineered asymmetry, *Nano Lett.* **16**, 1981 (2016).
- [35] Z. Wang, *et al.*, Thermal generation, manipulation and thermoelectric detection of skyrmions, *Nat. Electron.* **3**, 672 (2020).

- [36] K. Litzius, J. Leliaert, P. Bassirian, D. Rodrigues, S. Kromin, I. Lemesh, J. Zazvorka, K.-J. Lee, J. Mulders, N. Kerber, D. Heinze, N. Keil, R. M. Reeve, M. Weigand, B. Van Waeyenberge, G. Schütz, K. Everschor-Sitte, G. S. D. Beach, and M. Kläui, The role of temperature and drive current in skyrmion dynamics, *Nat. Electron.* **3**, 30 (2020).
- [37] C. Schutte, J. Iwasaki, A. Rosch, and N. Nagaosa, Inertia, diffusion, and dynamics of a driven skyrmion, *Phys. Rev. B* **90**, 174434 (2014).
- [38] R. E. Troncoso and Á. S. Núñez, Brownian motion of massive skyrmions in magnetic thin films, *Ann. Phys.* **351**, 850 (2014).
- [39] R. Tomasello, M. Ricci, P. Burrascano, V. Puliafito, M. Carpentieri, and G. Finocchio, Electrical detection of single magnetic skyrmion at room temperature, *AIP Adv.* **7**, 056022 (2017).
- [40] R. Tomasello, K. Y. Guslienko, M. Ricci, A. Giordano, J. Barker, M. Carpentieri, O. Chubykalo-Fesenko, and G. Finocchio, Origin of temperature and field dependence of magnetic skyrmion size in ultrathin nanodots, *Phys. Rev. B* **97**, 060402 (2018).
- [41] R. Tomasello, A. Giordano, S. Chiappini, R. Zivieri, G. Siracusano, V. Puliafito, I. Medlej, A. La Corte, B. Azzerboni, M. Carpentieri, Z. Zeng, and G. Finocchio, micromagnetic understanding of the skyrmion Hall angle current dependence in perpendicularly magnetized ferromagnets, *Phys. Rev. B* **98**, 224418 (2018).
- [42] J. Zázvorka, F. Jakobs, D. Heinze, N. Keil, S. Kromin, S. Jaiswal, K. Litzius, G. Jakob, P. Virnau, D. Pinna, K. Everschor-Sitte, L. Rózsa, A. Donges, U. Nowak, and M. Kläui, Thermal skyrmion diffusion used in a reshuffler device, *Nat. Nanotechnol.* **14**, 658 (2019).
- [43] D.-J. Kim, C.-Y. Jeon, J.-G. Choi, J. W. Lee, S. Surabhi, J.-R. Jeong, K.-J. Lee, and B.-G. Park, Observation of transverse spin Nernst magnetoresistance induced by thermal spin current in ferromagnet/non-magnet bilayers, *Nat. Commun.* **8**, 1400 (2017).
- [44] A. A. Kovalev and Y. Tserkovnyak, Thermoelectric spin transfer in textured magnets, *Phys. Rev. B* **80**, 100408 (2009).
- [45] L. Kong and J. Zang, Dynamics of an Insulating Skyrmion under a Temperature Gradient, *Phys. Rev. Lett.* **111**, 067203 (2013).
- [46] C. Gong, Y. Zhou, and G. Zhao, Dynamics of magnetic skyrmions under temperature gradients, *Appl. Phys. Lett.* **120**, 052402 (2022).
- [47] R. Tomasello, S. Komineas, G. Siracusano, M. Carpentieri, and G. Finocchio, Chiral skyrmions in an anisotropy gradient, *Phys. Rev. B* **98**, 024421 (2018).
- [48] A. A. Thiele, Steady-State Motion of Magnetic Domains, *Phys. Rev. Lett.* **30**, 230 (1973).
- [49] N. K. Duong, R. Tomasello, M. Raju, A. P. Petrović, S. Chiappini, G. Finocchio, and C. Panagopoulos, Magnetization reversal signatures of hybrid and pure Néel skyrmions in thin film multilayers, *APL Mater.* **8**, 111112 (2020).
- [50] F. Schlickeiser, U. Ritzmann, D. Hinzke, and U. Nowak, Role of Entropy in Domain Wall Motion in Thermal Gradients, *Phys. Rev. Lett.* **113**, 097201 (2014).
- [51] X. Zhang, Y. Zhou, and M. Ezawa, Magnetic bilayer-skyrmions without skyrmion Hall effect, *Nat. Commun.* **7**, 10293 (2016).
- [52] R. Tomasello, V. Puliafito, E. Martinez, A. Manchon, M. Ricci, M. Carpentieri, and G. Finocchio, Performance of synthetic antiferromagnetic racetrack memory: Domain wall versus skyrmion, *J. Phys. D: Appl. Phys.* **50**, 325302 (2017).
- [53] R. Tomasello, A. Giordano, F. Garescì, G. Siracusano, S. De Caro, C. Ciminelli, M. Carpentieri, and G. Finocchio, Role of magnetic skyrmions for the solution of the shortest path problem, *J. Magn. Magn. Mater.* **532**, 167977 (2021).
- [54] A. Giordano, G. Finocchio, L. Torres, M. Carpentieri, and B. Azzerboni, Semi-implicit integration scheme for Landau-Lifshitz-Gilbert-Slonczewski equation, *J. Appl. Phys.* **111**, 07D112 (2012).
- [55] L. Lopez-Diaz, D. Aurelio, L. Torres, E. Martinez, M. a Hernandez-Lopez, J. Gomez, O. Alejos, M. Carpentieri, G. Finocchio, and G. Consolo, Micromagnetic simulations using graphics processing units, *J. Phys. D: Appl. Phys.* **45**, 323001 (2012).
- [56] R. Tomasello, M. Carpentieri, and G. Finocchio, Influence of the Dzyaloshinskii-Moriya interaction on the spin-torque diode effect, *J. Appl. Phys.* **115**, 17C730 (2014).
- [57] *Spintronics-Based Computing*, edited by W. Zhao and G. Prenat (Springer International Publishing, Cham, 2015).
- [58] K.-M. Lee, J. W. Choi, J. Sok, and B.-C. Min, Temperature dependence of the interfacial magnetic anisotropy in W/CoFeB/MgO, *AIP Adv.* **7**, 065107 (2017).
- [59] E. Grimaldi, V. Krizakova, G. Sala, F. Yasin, S. Couet, G. Sankar Kar, K. Garello, and P. Gambardella, Single-shot dynamics of spin-orbit torque and spin transfer torque switching in three-terminal magnetic tunnel junctions, *Nat. Nanotechnol.* **15**, 111 (2020).
- [60] See Supplemental Material at <http://link.aps.org/supplemental/10.1103/PhysRevApplied.18.024062> for the micromagnetic parameters, the details of the generalized Thiele's equation, the effect of the gradient of each parameter on the skyrmion motion in a single-layer FM, the effect of the gradient amplitude, and the effect of the magnonic torque.
- [61] R. Tomasello, E. Martinez, R. Zivieri, L. Torres, M. Carpentieri, and G. Finocchio, A strategy for the design of skyrmion racetrack memories, *Sci. Rep.* **4**, 6784 (2014).
- [62] M. Björck, M. Hedlund, and G. Andersson, Magnetic moments in Fe-Co/Pt superlattices, *J. Magn. Magn. Mater.* **320**, 2660 (2008).
- [63] P. Asselin, R. F. L. Evans, J. Barker, R. W. Chantrell, R. Yanes, O. Chubykalo-Fesenko, D. Hinzke, and U. Nowak, Constrained Monte Carlo method and calculation of the temperature dependence of magnetic anisotropy, *Phys. Rev. B* **82**, 054415 (2010).
- [64] U. Atxitia, D. Hinzke, O. Chubykalo-Fesenko, U. Nowak, H. Kachkachi, O. N. Mryasov, R. F. Evans, and R. W. Chantrell, Multiscale modeling of magnetic materials: Temperature dependence of the exchange stiffness, *Phys. Rev. B* **82**, 134440 (2010).
- [65] L. Rózsa, U. Atxitia, and U. Nowak, Temperature scaling of the Dzyaloshinsky-Moriya interaction in the spin wave spectrum, *Phys. Rev. B* **96**, 094436 (2017).
- [66] R. Moreno, R. F. L. Evans, S. Khmelevskyi, M. C. Muñoz, R. W. Chantrell, and O. Chubykalo-Fesenko, Temperature-dependent exchange stiffness and domain wall width in Co, *Phys. Rev. B* **94**, 104433 (2016).

- [67] B. F. McKeever, D. R. Rodrigues, D. Pinna, A. Abanov, J. Sinova, and K. Everschor-Sitte, Characterizing breathing dynamics of magnetic skyrmions and antiskyrmions within the hamiltonian formalism, *Phys. Rev. B* **99**, 054430 (2019).
- [68] K. Everschor, M. Garst, R. A. Duine, and A. Rosch, Current-induced rotational torques in the skyrmion lattice phase of chiral magnets, *Phys. Rev. B* **84**, 064401 (2011).
- [69] K. Everschor-Sitte and M. Sitte, Real-space Berry phases: Skyrmion soccer (Invited), *J. Appl. Phys.* **115**, 172602 (2014).
- [70] S. Rohart and A. Thiaville, Skyrmion confinement in ultrathin film nanostructures in the presence of Dzyaloshinskii-Moriya interaction, *Phys. Rev. B* **88**, 184422 (2013).
- [71] R. Zivieri, R. Tomasello, O. Chubykalo-Fesenko, V. Tiberkevich, M. Carpentieri, and G. Finocchio, Configurational entropy of magnetic skyrmions as an ideal gas, *Phys. Rev. B* **99**, 174440 (2019).
- [72] F. Büttner, I. Lemesh, and G. S. D. Beach, Theory of isolated magnetic skyrmions: From fundamentals to room temperature applications, *Sci. Rep.* **8**, 4464 (2018).
- [73] S. Tacchi, R. E. Troncoso, M. Ahlberg, G. Gubbiotti, M. Madami, J. Åkerman, and P. Landeros, Interfacial Dzyaloshinskii-Moriya Interaction in Pt/CoFeB Films: Effect of the Heavy-Metal Thickness, *Phys. Rev. Lett.* **118**, 147201 (2017).
- [74] W. Legrand, J.-Y. Chauleau, D. Maccariello, N. Reyren, S. Collin, K. Bouzehouane, N. Jaouen, V. Cros, and A. Fert, Hybrid chiral domain walls and skyrmions in magnetic multilayers, *Sci. Adv.* **4**, eaat0415 (2018).
- [75] W. F. Brown, Thermal fluctuations of a single-domain particle, *Phys. Rev.* **130**, 1677 (1963).
- [76] G. Finocchio, I. N. Krivorotov, X. Cheng, L. Torres, and B. Azzerboni, Micromagnetic understanding of stochastic resonance driven by spin-transfer-torque, *Phys. Rev. B* **83**, 134402 (2011).
- [77] S. S. P. Parkin and D. Mauri, Spin engineering: Direct determination of the Ruderman-Kittel-Kasuya-Yosida far-field range function in ruthenium, *Phys. Rev. B* **44**, 7131 (1991).
- [78] S.-H. Yang, K.-S. Ryu, and S. Parkin, Domain-wall velocities of up to  $750 \text{ ms}^{-1}$  driven by exchange-coupling torque in synthetic antiferromagnets, *Nat. Nanotechnol.* **10**, 221 (2015).
- [79] S. Karayev, P. D. Murray, D. Khadka, T. R. Thapaliya, K. Liu, and S. X. Huang, Interlayer exchange coupling in Pt/Co/Ru and Pt/Co/Ir superlattices, *Phys. Rev. Mater.* **3**, 041401 (2019).
- [80] R. A. Duine, K.-J. Lee, S. S. P. Parkin, and M. D. Stiles, Synthetic antiferromagnetic spintronics, *Nat. Phys.* **14**, 217 (2018).